Comparison of thermionic filament and carbon nanotube field emitter-based electron ionization sources in cycloidal coded aperture mass analyzers

Raul Vyas[a], Philip J. Herr[a], Tanouir Aloui[a], Kathleen Horvath[a], Matthew P. Kirley[a], Charles B. Parker[a], Adam D. Keil[b], James B. Carlson[c], Justin Keogh[d], Roger P. Sperline[d], M. Bonner Denton[d], M. Luisa Sartorelli[a,e], Brian R. Stoner[a], Michael E. Gehm[a], Jeffrey T. Glass[a], Jason J. Amsden[a,^]

Author Affiliations:

[a] Department of Electrical and Computer Engineering, 100 Science Drive, Duke University, Durham, NC, USA 27708

[b] Broadway Analytical, LLC, 1030 E. Harlem Avenue, Monmouth, IL, USA 61462

[c] Electronics and Applied Physics Division, 3040 E. Cornwallis Rd., RTI International, Research Triangle Park, Durham, NC, USA 27709

[d] Department of Chemistry and Biochemistry, 1306 E. University Blvd., University of Arizona, Tucson, AZ USA 85721

[e] Departamento de Física, Universidade Federal de Santa Catarina, Campus Universitário Trindade, Florianópolis, SC BRAZIL 88040-000

^Corresponding Author:

Jason J. Amsden

Department of Electrical and Computer Engineering

Duke University

Durham, NC 27708

(919)660-5592

jason.amsden@duke.edu

Abstract

This work compares the coded aperture imaging performance of thermionic filament and carbon nanotube (CNT) field emitter-based electron sources in cycloidal-coded aperture mass spectrometers. The use of spatially coded apertures in mass spectrometry enables miniaturization by improving throughput without sacrificing resolution. CNT-based electron ionization sources for mass spectrometers provide several potential benefits over conventional thermionic emitters, including low voltage and low power consumption, room temperature operation, long lifetime, and ability to emit electrons in a pulsed mode. However, spatiotemporal variation in electron emission from CNTs is a major disadvantage. In this study, electron emission stability and spatiotemporal stability of the coded aperture image were compared for coded aperture cycloidal mass analyzers with either a CNT-based ion source or a thermionic filament-based ion source. We found that the thermionic filament-based ion source produced a significantly more stable coded aperture image than the CNT based ion source. The aperture image fluctuations in the CNT-based source are likely a result of adsorption and desorption of molecules on the CNT surface that cause local work function changes and induce spatiotemporal variation in electron emission and subsequent ion generation.

Keywords: Carbon Nanotubes, Field Emission, Thermionic Filament, Coded Apertures, Cycloidal Mass Analyzer

1 Introduction

Miniature mass spectrometers find use in a wide variety of potential applications including environmental monitoring [1-4], protein characterization [5, 6], and space exploration [7, 8]. Most miniature mass spectrometers are based on quadrupole or ion trap mass analyzers [9-11]. However, with the development and incorporation of three key technologies: neodymium-iron-boron (Nd-Fe-B) permanent magnets [12, 13], ion array detectors [14-17], and spatial aperture coding in mass spectrometry [18-21], there is interest in miniature sector instruments as they consume less power, offer simultaneous detection of ions over a wide mass range, and increase throughput without sacrificing resolution.

Shrinking sector mass spectrometers results in a trade-off between throughput and resolution [18, 23]. Replacing the traditional resolution defining slit in a magnetic sector mass spectrometer with an array of slits called a coded aperture can overcome this trade-off. The resulting coded spectrum has an image of the coded aperture projected on the detector for each mass to charge. The mass spectrum can be computationally reconstructed using a two-step approach. First, the system response function is estimated from the coded spectrum of a known compound. Second, the reconstructed spectrum is obtained by a deconvolution of the estimated system response from the coded spectrum for an unknown compound or compounds [23]. In the last decade, aperture coding has been demonstrated in 90˚ magnetic sector [19, 20] and Mattauch-Herzog double-focusing [21] mass analyzers. More recently, a cycloidal coded aperture miniature mass

spectrometer (C-CAMMS) proof-of-concept instrument demonstrated over a ten-fold increase in throughput without a loss of resolution as compared with a single slit instrument. C-CAMMS also incorporated a carbon nanotube (CNT) field emission electron ionization source and a capacitive transimpedance amplifier (CTIA) array detector [18].

To take full advantage of spatial aperture coding and enable an accurate spectral reconstruction, the ion source must produce spatially and temporally uniform aperture images at the detector to ensure a constant system response. Historically, electron ionization has been used most commonly with mass spectrometers to create gas phase ions from a wide range of small molecules [11]. Electron sources used for electron ionization generally employ thermionic filaments because they offer stable electron emission. However, thermionic filaments have a high-power consumption, significant heat generation, short lifetimes at higher pressures, and an inability to be pulsed on and off frequently – all disadvantageous for fieldable mass spectrometry applications. CNT field emission sources have been demonstrated to be attractive potential alternatives to thermionic filaments in miniature mass spectrometers [24, 25]. CNTs show good electrical conductivity, high electric field tolerance, and chemical inertness [26-28]. Additionally, their low power consumption [24, 25, 29, 30], high current densities [31, 32], ability to switch on-off rapidly [18, 29, 33], longer lifetimes (especially at elevated pressures) [25, 34], and room temperature operation [33] are advantageous over thermionic sources in miniature mass spectrometry applications. However, a major

disadvantage with CNT electron emission is the spatiotemporal variation in emission current [35-37].

This paper compares the aperture imaging performance of a CNT field emission-based ion source to a traditional thermionic emission-based ion source in cycloidal coded aperture miniature mass spectrometers with CTIA array detectors. In particular, we examine how the stability of CNT electron emission affects the aperture imaging performance compared to that of thermionic emission.

2 Materials and Methods

There are two miniature mass spectrometers used in this study, C-CAMMS-CNT which uses a CNT field emission-based source, and C-CAMMS-TF which uses a thermionic filament (TF)-based source. Both systems are largely based on the previous C-CAMMS instrument described in reference [18]. Key differences between the ion sources, cycloid mass analyzers, and vacuum systems in C-CAMMS-CNT and C-CAMMS-TF are described in the following sections. Other major components including the inlet, array detector, and the control electronics used in C-CAMMS-CNT and C-CAMMS-TF are the same as those used in the previous C-CAMMS instrument [18].

2.1 Mass Analyzer

The cycloidal mass analyzer design for both systems consists of a permanent magnet magnetic sector and an array of electrodes for the electric sector. The magnetic sector

(flux density - 0.3 T) used in both systems has an opposed dipole design as described previously [18, 38]. The electric sectors in both systems are comprised of 25 electrodes that are 3 mm tall and separated by 0.5 mm, creating an L-shaped box. To generate the desired electric field, C-CAMMS-CNT uses a printed circuit board (PCB) electric sector in the form of an L-shaped hollow box with an internal cavity 12.9 mm deep, 84.9 mm tall, 75.9 mm wide at the base of the L, and 42.4 mm wide towards the top of the L. The ion sources in the electric sectors of C-CAMMS-CNT and C-CAMMS-TF are placed midway between two center electric sector electrodes, rather than in-line with the grounded electrode as was done in the previous C-CAMMS instrument [18]. Landry et al. determined that this configuration produced a more uniform electric field and an improved aperture imaging quality [38]. The electric sector electrodes in C-CAMMS-CNT are fabricated as gold tracks on the inner surface of a 1 mm thick 370HR (Isola) circuit board. The circuit board was fabricated to conform to IPC-A-600 Class 2 specifications. The IPC-A-600 Class 2 standard is a specification for acceptability requirements for the circuit board. It is not intended to be used as a performance specification for printed board manufacture, but rather sets the criteria for an acceptable quality of board based on a visual inspection process. These visual indicators ensure that the quality and performance repeatability are maintained. The gold tracks were fabricated from 1-ounce copper with a plating finish of electroless nickel immersion gold per IPC-4552 specifications, similar to the previous C-CAMMS instrument [18]. C-CAMMS-TF uses machined aluminum electrodes in place of a circuit board electric sector electrodes, arranged to form an electric sector retaining the L-shape with an internal cavity 15 mm deep, 84 mm tall, 78 mm wide at the base of the L, and 45.5 mm wide toward the top of

the L. These electrodes enable more precise alignment of the ion source, detector, and mass analyzer focal plane. These aluminum electrodes are sputter coated with a layer of titanium and gold to reduce surface charge collection and are separated by ceramic spacers. Further details on the construction of C-CAMMS-TF will be provided in a forthcoming publication. In particular, C-CAMMS-TF will have improved resolution over C-CAMMS-CNT due to an improved alignment of the coded aperture and the detector with the mass analyzer focal plane. However, none of the differences in the mass analyzers in C-CAMMS-CNT and C-CAMMS-TF are expected to result in a temporal change in the coded aperture image as observed in C-CAMMS-CNT.

2.2 Ion Source

The CNT field emission-based ion source in C-CAMMS-CNT is a standalone entity similar to the miniature ion source described in [18]. Figures 1 (a), (b), (c), (d), and (h) depict the ion source in C-CAMMS-CNT and some of its components, including CNT-based electron sources, the ion repeller box, and the apertures. A low temperature co-fired ceramic (LTCC) scaffold (pictured in Figure 1 (b)) houses the CNT electron sources, an ion repeller, an extraction aperture, and a coded aperture. The electron source is a vertically aligned multi-walled CNT array grown in an etched cavity on a silicon wafer. The ion repeller is constructed using an electroformed metal box with grids on opposing sides. The grids direct transmission of electrons from the CNT sources into the center of the ion repeller. The ion repeller in C-CAMMS-CNT is wider than the one in the previous C-CAMMS instrument by 1.9 mm (increasing from 2.6 mm to 4.5 mm in width). A wider ion repeller reduces angular dispersion of the ion beam by reducing

curvature in the equipotential lines, resulting in ion trajectories with less angular dispersion. The extraction aperture directs the ions out of the ion source, and the coded aperture acts as a spatial filter for the ion beam.

The thermionic emission-based ion source in C-CAMMS-TF is placed in a specially designed cavity within the electric sector electrodes to improve alignment and the depth-of-focus. Figures 1 (e), (f), (g) and (h) show a cross-section of the thermionic filament-based source in C-CAMMS-TF and some of its key components, where (e) is a cross-section of the source, (f) shows the filament and the repeller together, and (g) is the filament. The thermionic source is an yttria-coated iridium filament housed in a Vespel body (Scientific Instrument Services, Inc.). A thinner filament compared to the height of the CNT array reduces the potential gradient over which ions are generated, resulting in lower energy dispersion. The ion repeller box is 5 mm wide, compared to the 4.5 mm wide C-CAMMS-CNT ion repeller which further reduces the angular dispersion of the ion beam. The ion repeller box is constructed out of titanium and plated in gold to reduce surface charge accumulation [39]. The extraction aperture was not included as part of the C-CAMMS-TF ion source as simulations indicated it had a minimal effect on the shape of the equipotential lines inside the ion source and therefore little effect on directing the ions out of the ion source [18].

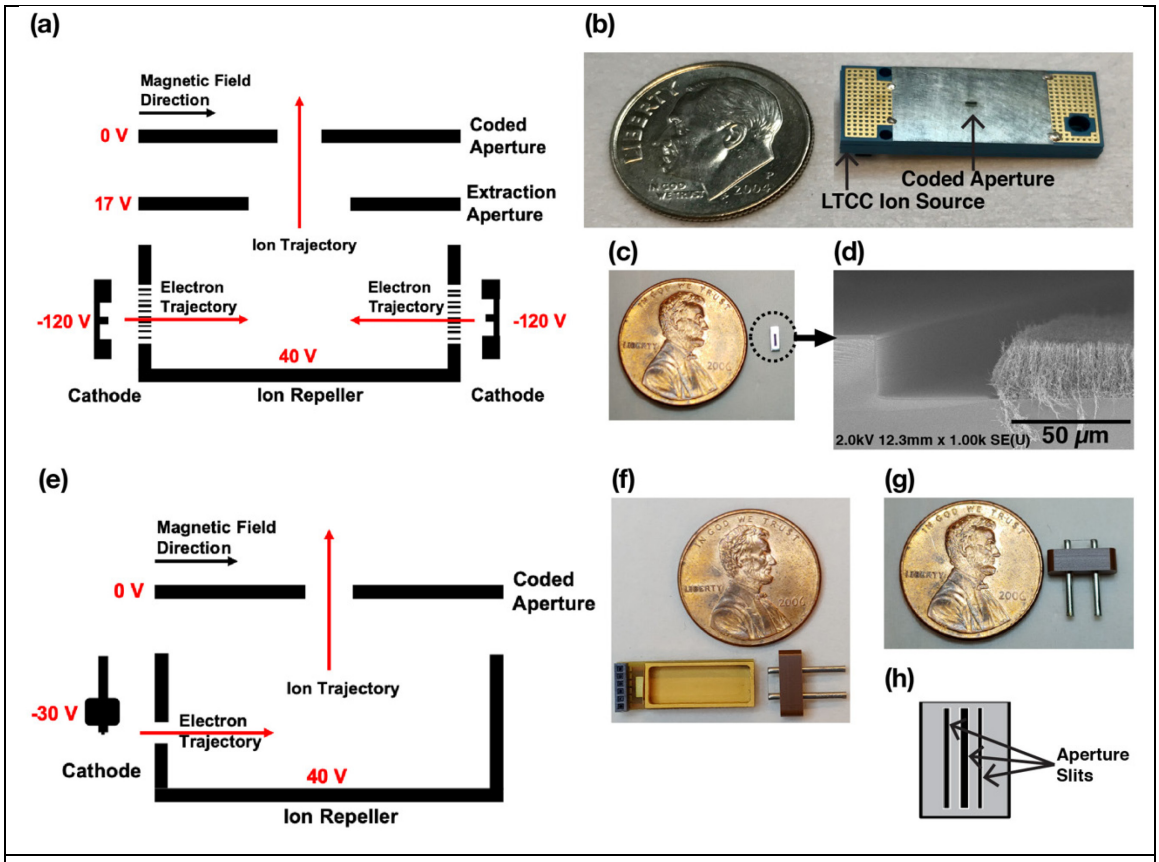

Figure 1: Ion sources used in C-CAMMS-CNT and C-CAMMS-TF.
(a), (b), (c) and (d) depict the ion source in C-CAMMS-CNT, where (a) is a cross-section of the source, (b) is the assembled LTCC ion source, (c) is the CNT chip, and (d) is a scanning electron microscope image of a cross-section of the carbon nanotube emitters; (e), (f) and (g) show a cross-section of the thermionic filament-based source in C-CAMMS-TF and some of its key components, where (e) is a cross-section of the source, (f) shows the filament and the repeller together, (g) is the filament; and (h) is a schematic of the coded aperture used in both C-CAMMS-CNT and C-CAMMS-TF.

3 Results

3.1 Electron emission comparison

Figure 2 shows a comparison of the electron emission current over time for the CNT chip vs. the filament. Vacuum for both ion sources was held at a chamber pressure of approximately 1.3×10^{-5} mbar. The voltages for the ion repeller, filament float, CNT chips and the apertures were supplied and controlled by Keithley 2410 source meters. The

filament was powered by an Agilent 3640A DC power supply. The CNTs' electron emission stability over time was obtained by collecting the emission current at a fixed potential difference of 160 V between the ion repeller and the CNT chip over a 30 min. period. The potential on the CNT chip was selected to be -120 V relative to 40 V on the ion repeller to match the potential difference between them required for field emission from the CNTs. The filament electron emission stability over time was obtained by collecting the emission current at a constant potential difference of 70 V between the repeller and the filament. The filament was floated at a potential of -30V relative to 40 V on the ion repeller to produce 70 eV electrons (Figure 1(e)). Achieving 400 nA of emission current from the filament required a potential difference of 1.1 V across the filament with 1.5 A of current running through the filament. From Figure 2, electron current from the CNTs was observed to be 130±60 nA, whereas the electron current from the heated filament was determined to be 400±3 nA, clearly demonstrating higher emission stability (electron current is expressed as: mean ± standard deviation). There are several potential methods to improve current stability in CNT field emitters which are discussed in Section 4.

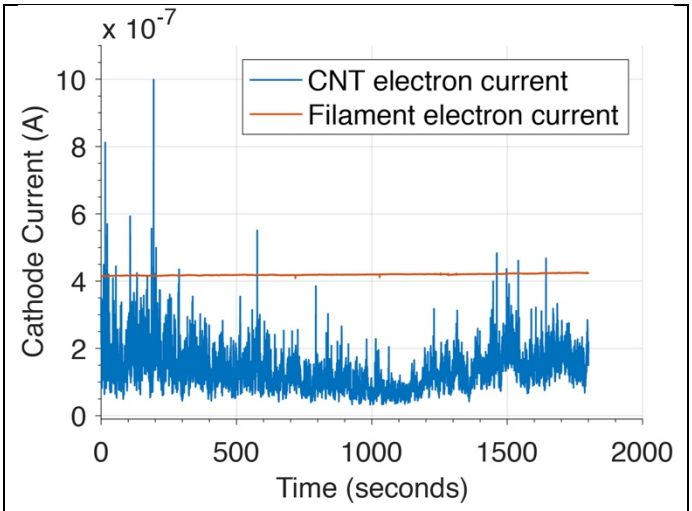

Figure 2. Electron emission current comparison. A comparison of electron emission current for CNTs vs. a thermionic filament over time, demonstrating a more stable emission current from the filament.

3.2 Coded aperture imaging performance

To compare the aperture imaging performance of the CNT and thermionic filament-based ion sources, the stability of the aperture image of singly ionized argon was observed over time for C-CAMMS-CNT and C-CAMMS-TF. Figures 3 (a) and (b) compare several coded aperture images of singly ionized argon (Ar^+ at m/z 40) taken with each instrument over a two second duration. The aperture uses a pattern consisting of three slits: 100 µm, 150 µm, and 50 µm wide, separated by 100 µm and 150 µm respectively. In each figure, an ideal coded aperture image is shown in grey behind the experimental data in blue. As discussed in the C-CAMMS paper, the difference between the ideal image and the experimental image is due to alignment and field uniformity [18]. An improved definition of peaks corresponding to each of the aperture images for C-CAMMS-TF in Figure 3 (b) also indicates an improvement in resolution over the aperture images for C-CAMMS-

CNT in Figure 3 (a). The improvement in resolution can be attributed to improvements in alignment, as discussed in Section 2.1.

Note that the peak height corresponding to each slit of the coded aperture image in Figure 3 (a) for C-CAMMS-CNT varies more with time compared to Figure 3 (b) for C-CAMMS-TF. To further investigate and characterize this variation, the data for the Ar^+ coded aperture image was collected over a duration of 100 seconds. Figures 3 (c) and (d) compare the relative intensity of each peak of the coded aperture image (corresponding to the 100, 150, and 50 μm slits of the aperture) over a period of 100 seconds for C-CAMMS-CNT and C-CAMMS-TF. From the plots, it is clear that there is a large variation in peak height over time for each slit of the coded aperture image for Ar^+ with C-CAMMS-CNT (Figure 3 (c)) compared to C-CAMMS-TF (Figure 3(d)). These data indicate that the aperture image for C-CAMMS-CNT is less stable than the aperture image for C-CAMMS-TF. The potential causes behind the aperture image variation in C-CAMMS-CNT are discussed in detail in the next section.

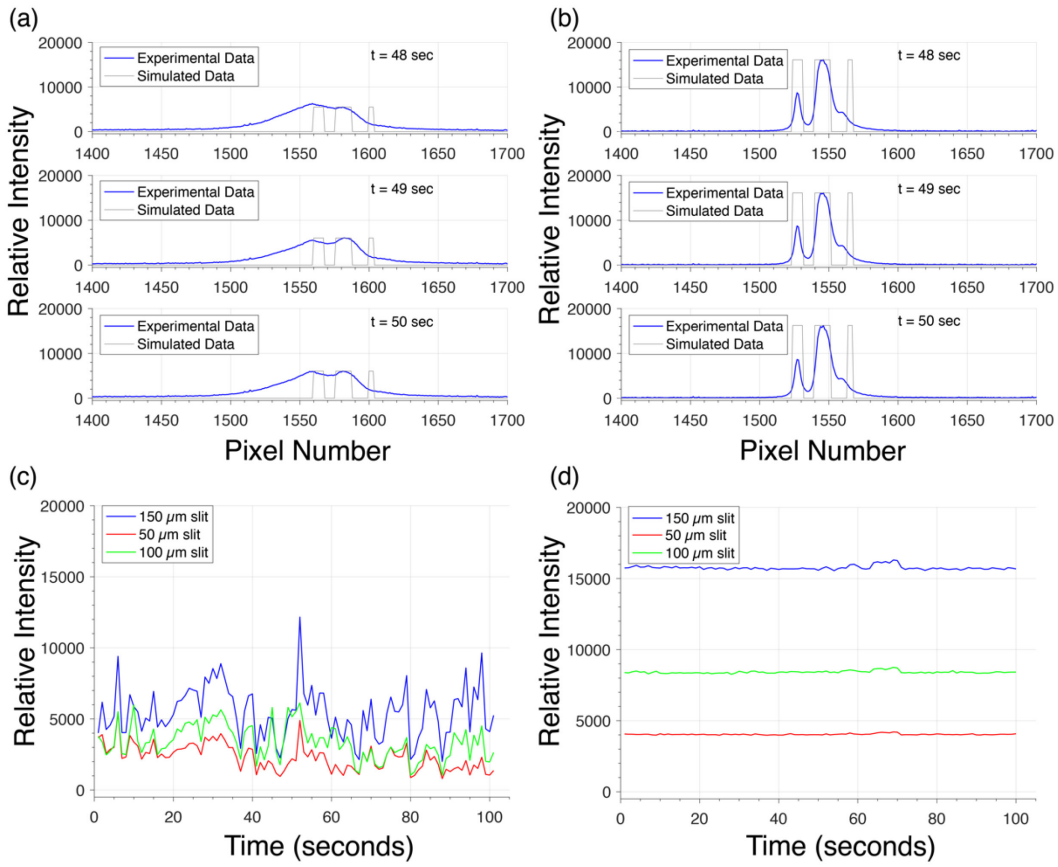

Figure 3. A comparison of coded aperture image stability and resolution performance.
(a) Aperture image for Ar^+ (m/z – 40) obtained over time over a period of two seconds with CNT-based, vs. (b) thermionic filament-based ion source; the grey trace is the simulated coded aperture image for Ar^+, (c) relative intensity of each peak of the aperture image for Ar^+ (m/z – 40) over time for CNT-based, vs. (d) thermionic filament-based ion source.

4 Discussion and Conclusion

The data in Figure 3 demonstrate that the coded aperture image stability is much worse in C-CAMMS-CNT than in C-CAMMS-TF. The stable coded aperture image in C-CAMMS-TF will ensure a constant system response and improved spectral reconstruction quality. The variation in the coded aperture image in C-CAMMS-CNT could be a result of spatiotemporal fluctuations in the ion current, as seen from Figure 3

(c). These variations in ion current could stem from a spatiotemporal variation in electron emission from the CNTs [40]. Figure 2 also supports this hypothesis by providing evidence of a noisier electron emission from the CNTs compared to thermionic emission.

The Fowler-Nordheim (FN) equation [43] that describes field emission from a planar surface provides insights into the cause of spatiotemporal variation in field emission from carbon nanotube films such as those used in C-CAMMS-CNT, and the resultant variation in ion current and coded aperture image. The FN equation indicates that the emission current is proportional to the local electric field F and work function ϕ (1). The presence of a high local electric field enhances field emission from the CNTs.

$$J \propto \frac{\left(F^2\right)}{\phi} \exp\left(\frac{-\phi^{3/2}}{F}\right) \tag{1}$$

Since the emission current is an exponential function of F and $\phi^{3/2}$, small changes in either quantity result in large changes in emitted current. Changes in the emitter tip geometry due to ion bombardment and/or surface migration of atoms in the presence of a high field cause variations in F [35, 44]. However, for CNTs the impact of ion bombardment is minimal due to the low sputter coefficient of carbon [45], and the crystalline covalent structure of a CNT makes surface migration at the CNT tip also unlikely due to the high activation energy needed for the removal of a sp^2 bonded carbon atom [35, 46].

Adsorption and desorption of gases on the surface of the CNTs can cause as much as 20% variation in ϕ, resulting in almost two orders of magnitude change in emitted current [35, 47-49]. Molecules continually adsorbing and desorbing from different locations on the surface of the CNTs and changing the work function and emission current in these constantly varying locations will result in spatiotemporal variations in the emission of electrons from the CNTs. It is also possible that the strong 0.3 T magnetic field could cause some variation in the CNT emission current [50]. However, with our CNTs, we see a similar variation in emission current both with and without a magnetic field present (data not shown), so the adsorption and desorption of gases changing the work function is likely the dominant mechanism causing current fluctuations. For a uniform illumination of the aperture and a stable image of the aperture at the detector, the ionization volume defined by the electron trajectories needs to be wider (widths w_1, w_2, *and* w_3 in Figure 4) than the width of the open area of the aperture (width w in Figure 4). A spatiotemporal variation in the ionization volume and the resultant ion trajectories will lead to a non-uniform illumination of the aperture, affecting the aperture image stability. Figure 4 demonstrates how a spatial variation in electron emission from CNTs at three different times t_1, t_2 and t_3 can cause a spatiotemporal variation in ionization volume and ion trajectories, resulting in a non-uniform illumination of the aperture each time. In Figure 4, the electron trajectories (coming out of the page) are colored in red, blue and yellow, to signify the spatiotemporal variation caused by random adsorption and/or desorption processes occurring in different locations at different times. This spatiotemporal variation in electron trajectories leads to a spatiotemporal variation in the ionization volume and ion trajectories (also with matching red, blue and yellow colors denoting a correlation

between the spatiotemporal variation in electron trajectories and ion trajectories). Since each of the ionization volumes defined by the electron trajectories is narrower than the total aperture open area width, the spatiotemporal variation in the ion trajectories will cause a non-uniform illumination of the coded aperture as a function of time. In contrast, the high operating temperatures of the thermionic filament could make the adsorption of gases on the filament surface less likely, minimizing work function changes [51] and subsequent spatial variations in thermionic current. The aperture image with C-CAMMS-TF containing a thermionic filament-based ion source is more stable, resulting from the more stable and uniform (i.e., with a less spatiotemporal variation) volume of electrons providing a spatially uniform ionization current.

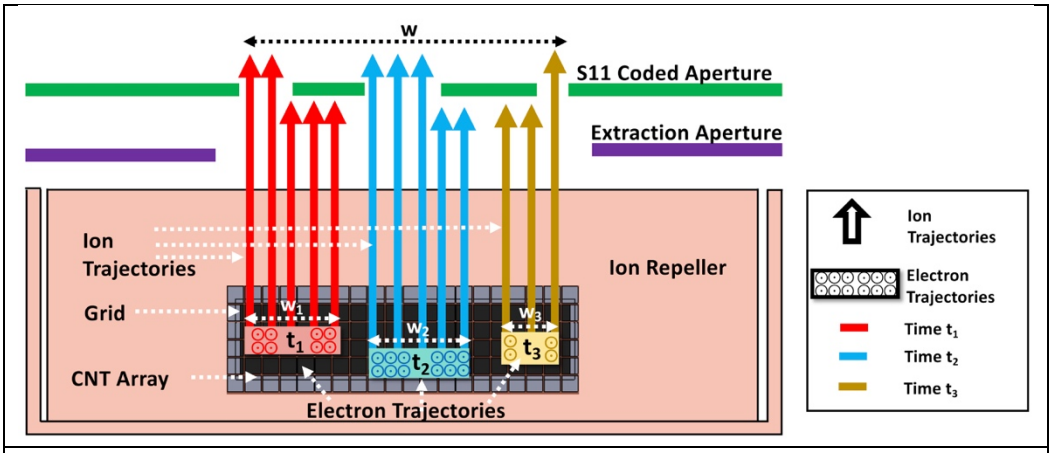

Figure 4. Explanation for non-uniform illumination of aperture in C-CAMMS-CNT. Cross section view of C-CAMMS-CNT ion source, illustrating a spatial variation in electron emission from CNTs at three different times t_1, t_2 and t_3. This spatiotemporal variation in electron trajectories leads to a spatiotemporal variation in the ionization volume and ion trajectories. Since each of the ionization volumes defined by the electron trajectories is narrower than the total aperture open area width, the spatiotemporal variation in the ion trajectories will cause a non-uniform illumination of the coded aperture as a function of time.

There are several potential methods to improve the spatiotemporal emission stability of CNTs. Reports have suggested that a joule heating of the CNTs will prevent adsorption

and desorption of gases on their surface, preventing work function changes [35, 52]. However, the additional power requirements may make heating the CNTs impractical in some fieldable applications such as those targeting space exploration, flat-panel displays, and vacuum microelectronics. In addition, several studies have indicated that the stability of field emission from CNTs can be increased by encapsulating them in an insulator to reduce electric field screening effects and polishing the surface to ensure a homogeneous length for the CNTs [37, 53, 54]. Moreover, a recent report suggests that sputter-coated titanium may prevent the contamination of the CNT surface by residual vacuum chamber gases [55].

In conclusion, this paper presented a comparison of CNT field emission-based and thermionic filament-based ion sources, used with cycloidal coded aperture miniature mass spectrometers. It was determined that spatiotemporal variation in electron emission from CNTs can result in a non-uniform illumination of the coded aperture. In contrast, spatiotemporally uniform thermionic emission of electrons from a heated filament provides an ideal volume of ions for uniform illumination of the aperture.

5 Acknowledgments

The authors would like to thank Dr. Elettra Piacentino for her assistance in proof-reading this article.

Funding: The information, data, or work presented herein were funded in part by the Advanced Research Projects Agency-Energy (ARPA-E), U.S. Department of Energy, under Award Number DE- AR0000546 and the National Science Foundation under Award Number 1632069. The views and opinions of authors expressed herein do not necessarily state or reflect those of the United States Government or any agency thereof.

6 References

1. Bell, R.J., et al., *A field-portable membrane introduction mass spectrometer for real-time quantitation and spatial mapping of atmospheric and aqueous contaminants.* Journal of The American Society for Mass Spectrometry, 2015. **26**(2): p. 212-223.
2. Keil, A., et al., *Monitoring of toxic compounds in air using a handheld rectilinear ion trap mass spectrometer.* Analytical Chemistry, 2008. **80**(3): p. 734-741.
3. Camilli, R., et al., *Tracking hydrocarbon plume transport and biodegradation at Deepwater Horizon.* Science, 2010. **330**(6001): p. 201-204.
4. Mach, P.M., et al., *A portable mass spectrometer study targeting anthropogenic contaminants in Sub-Antarctic Puerto Williams, Chile.* International Journal of Mass Spectrometry, 2017. **422**: p. 148-153.
5. Hou, C., et al., *Toward high pressure miniature protein mass spectrometer: Theory and initial results.* Journal of Mass Spectrometry, 2019.
6. Li, L., et al., *Mini 12, Miniature Mass Spectrometer for Clinical and Other Applications□ Introduction and Characterization.* Analytical Chemistry, 2014. **86**(6): p. 2909-2916.
7. Ren, Z., et al., *A review of the development and application of space miniature mass spectrometers.* Vacuum, 2018. **155**: p. 108-117.
8. Arevalo Jr, R., Z. Ni, and R.M. Danell, *Mass spectrometry and planetary exploration: A brief review and future projection.* Journal of Mass Spectrometry, 2020. **55**(1): p. e4454.
9. Badman, E.R. and R. Graham Cooks, *Miniature mass analyzers.* Journal of Mass Spectrometry, 2000. **35**(6): p. 659-671.
10. Ouyang, Z. and R.G. Cooks, *Miniature Mass Spectrometers.* Annual Review of Analytical Chemistry, 2009. **2**(1): p. 187-214.
11. Maher, S., F.P. Jjunju, and S. Taylor, *Colloquium: 100 years of mass spectrometry: Perspectives and future trends.* Reviews of Modern Physics, 2015. **87**(1): p. 113.
12. Herbst, J. and J. Croat, *Neodymium-iron-boron permanent magnets.* Journal of Magnetism and Magnetic Materials, 1991. **100**(1-3): p. 57-78.
13. Fraden, J., *Handbook of Modern Sensors*. Vol. 3. 2010: Springer.
14. Sinha, M.P. and M. Wadsworth, *Miniature focal plane mass spectrometer with 1000-pixel modified-CCD detector array for direct ion measurement.* Review of Scientific Instruments, 2005. **76**(2): p. 025103.
15. Hadjar, O., et al., *IonCCD™ for Direct Position-Sensitive Charged-Particle Detection: from Electrons and keV Ions to Hyperthermal Biomolecular Ions.* Journal of The American Society for Mass Spectrometry, 2011. **22**(4): p. 612-623.

16. Felton, J.A., et al., *Evaluation of a fourth-generation focal plane camera for use in plasma-source mass spectrometry.* Journal of Analytical Atomic Spectrometry, 2011. **26**(2): p. 300-304.
17. Schilling, G.D., et al., *Evaluation of a 512-Channel Faraday-Strip Array Detector Coupled to an Inductively Coupled Plasma Mattauch−Herzog Mass Spectrograph.* Analytical Chemistry, 2009. **81**(13): p. 5467-5473.
18. Amsden, J.J., et al., *Proof of concept coded aperture miniature mass spectrometer using a cycloidal sector mass analyzer, a carbon nanotube (CNT) field emission electron ionization source, and an array detector.* Journal of The American Society for Mass Spectrometry, 2018. **29**(2): p. 360-372.
19. Chen, E.X., et al., *Order of magnitude signal gain in magnetic sector mass spectrometry via aperture coding.* Journal of The American Society for Mass Spectrometry, 2015. **26**(9): p. 1633-1640.
20. Russell, Z.E., et al., *Two-dimensional aperture coding for magnetic sector mass spectrometry.* Journal of The American Society for Mass Spectrometry, 2015. **26**(2): p. 248-256.
21. Russell, Z.E., et al., *Compatibility of Spatially Coded Apertures with a Miniature Mattauch-Herzog Mass Spectrograph.* Journal of The American Society for Mass Spectrometry, 2016. **27**(4): p. 578-584.
22. Kogan, V., et al., *Design and testing of a portable magnetic mass spectrometer.* Field Analytical Chemistry & Technology, 1997. **1**(6): p. 331-342.
23. Amsden, J.J., et al., *Coded apertures in mass spectrometry.* Annual Review of Analytical Chemistry, 2017. **10**: p. 141-156.
24. Evans-Nguyen, T., et al., *Carbon Nanotube Electron Ionization Source for Portable Mass Spectrometry.* Analytical Chemistry, 2011. **83**(17): p. 6527-6531.
25. Radauscher, E.J., et al., *Chemical Ionization Mass Spectrometry Using Carbon Nanotube Field Emission Electron Sources.* Journal of The American Society for Mass Spectrometry, 2015. **26**(11): p. 1903-1910.
26. Bhushan, B., *Encyclopedia of nanotechnology*. 2012: Springer Dordrecht, Netherlands.
27. De Jonge, N. and J.M. Bonard, *Carbon nanotube electron sources and applications.* Philosophical Transactions of the Royal Society of London. Series A: Mathematical, Physical and Engineering Sciences, 2004. **362**(1823): p. 2239-2266.
28. Niyogi, S., et al., *Chemistry of single-walled carbon nanotubes.* Accounts of Chemical Research, 2002. **35**(12): p. 1105-1113.
29. Milne, W., et al., *Carbon nanotubes as field emission sources.* Journal of Materials Chemistry, 2004. **14**(6): p. 933-943.
30. Chen, L.Y., et al. *A Micro Ionizer for Portable Mass Spectrometers using Double-gated Isolated Vertically Aligned Carbon Nanofiber Arrays*. in *Electron Devices Meeting, 2007. IEDM 2007. IEEE International*. 2007.
31. Li, C., et al., *High emission current density, vertically aligned carbon nanotube mesh, field emitter array.* Applied Physics Letters, 2010. **97**(11): p. 113107.
32. Chernozatonskii, L., et al., *Electron field emission from nanofilament carbon films.* Chemical Physics Letters, 1995. **233**(1-2): p. 63-68.
33. Bower, C.A., et al., *On-chip electron-impact ion source using carbon nanotube field emitters.* Applied Physics Letters, 2007. **90**(12): p. 124102.
34. Bonard, J.-M., et al., *Field emission properties of multiwalled carbon nanotubes.* Ultramicroscopy, 1998. **73**(1-4): p. 7-15.

35. de Jonge, N., et al., *Low noise and stable emission from carbon nanotube electron sources.* Applied Physics Letters, 2005. **87**(13): p. 133118.
36. Kayastha, V.K., B. Ulmen, and Y.K. Yap, *Effect of graphitic order on field emission stability of carbon nanotubes.* Nanotechnology, 2007. **18**(3): p. 035206.
37. Pandey, A., et al., *Stable Electron Field Emission from PMMA− CNT Matrices.* Acs Nano, 2010. **4**(11): p. 6760-6766.
38. Landry, D.M., et al., *Effects of magnetic and electric field uniformity on coded aperture imaging quality in a cycloidal mass analyzer.* Journal of The American Society for Mass Spectrometry, 2018. **29**(2): p. 352-359.
39. D'Autry, W., et al., *Characterization and improvement of signal drift associated with electron ionization quadrupole mass spectrometry.* Analytical Chemistry, 2010. **82**(15): p. 6480-6486.
40. Halas, S. and T. Durakiewicz, *Techniques of ion current stabilization in isotope ratio mass spectrometry*, in *Handbook of Stable Isotope Analytical Techniques: Volume I*. 2004, Elsevier. p. 857-873.
41. Gaertner, G., *Historical development and future trends of vacuum electronics.* Journal of Vacuum Science & Technology B, Nanotechnology and Microelectronics: Materials, Processing, Measurement, and Phenomena, 2012. **30**(6): p. 060801.
42. Collins, C.M., *Ordered Nanomaterials for Electron Field Emission*. 2017, University of Cambridge.
43. Fowler, R.H. and L. Nordheim, *Electron emission in intense electric fields.* Proc. R. Soc. Lond. A, 1928. **119**(781): p. 173-181.
44. Hainfeld, J.F., *Understanding and using field emission sources*. 1977, Brookhaven National Lab., Upton, NY (USA).
45. Paulmier, T., et al., *Physico-chemical behavior of carbon materials under high temperature and ion irradiation.* Applied Surface Science, 2001. **180**(3-4): p. 227-245.
46. Crespi, V.H., et al., *Anisotropic electron-beam damage and the collapse of carbon nanotubes.* Physical Review B, 1996. **54**(8): p. 5927.
47. Kim, C., et al., *The effect of gas adsorption on the field emission mechanism of carbon nanotubes.* Journal of the American Chemical Society, 2002. **124**(33): p. 9906-9911.
48. Chen, C.-W. and M.-H. Lee, *Ab initio calculations of dimensional and adsorbate effects on the workfunction of single-walled carbon nanotube.* Diamond and related materials, 2003. **12**(3-7): p. 565-571.
49. Chen, C.-W., M.-H. Lee, and S. Clark, *Gas molecule effects on field emission properties of single-walled carbon nanotube.* Diamond and related materials, 2004. **13**(4-8): p. 1306-1313.
50. Bachtold, A., et al., *Aharonov–Bohm oscillations in carbon nanotubes.* Nature, 1999. **397**(6721): p. 673-675.
51. Greaves, W. and R. Stickney, *Adsorption studies based on thermionic emission measurements: III, oxygen on polycrystalline W, Mo, Ta, and Re.* Surface Science, 1968. **11**(3): p. 395-410.
52. Zhang, H., et al., *Performance of a Low Energy Ion Source with Carbon Nanotube Electron Emitters under the Influence of Various Operating Gases.* Nanomaterials, 2020. **10**(2): p. 354.
53. Lim, Y.D., et al., *Field emission properties of SiO2-wrapped CNT field emitter.* Nanotechnology, 2017. **29**(1): p. 015202.

54. Pandey, A., et al., *Very stable electron field emission from strontium titanate coated carbon nanotube matrices with low emission thresholds.* ACS nano, 2013. **7**(1): p. 117-125.
55. Zhang, H., et al., *Residual Gas Adsorption and Desorption in the Field Emission of Titanium-Coated Carbon Nanotubes.* Materials, 2019. **12**(18): p. 2937.